GEOLOGICA CARPATHICA, JUNE 2023, 74, 3, 233–244 https://doi.org/10.31577/GeolCarp.2023.13

Stress analysis from the southern part of Moravian Karst (Czech Republic)

JIŘÍ REZ[1,2,✉], MARKÉTA KERNSTOCKOVÁ[2] and VÍT BALDÍK[1]

[1]Czech Geological Survey, Leitnerova 22, 658 69 Brno, Czech Republic; ✉jura@eltekto.cz
[2]Department of Geological Sciences, Faculty of Science, Masaryk University, Kotlářská 2, 61137, Brno, Czech Republic

(Manuscript received December 28, 2022; accepted in revised form May 23, 2023; Associate Editor: Rastislav Vojtko)

Abstract: Data from three quarries in the southern Moravian Karst (SE Czech Republic), namely fault-slip data and calcite twinning data, enabled a side-to-side comparison of two paleostress analysis techniques. TwinCalc (www.eltekto.cz) was used to analyse 8 samples of calcite veins, yielding 20 stress states and MARK was used to analyse the fault-slip data yielding 10 stress states. 26 out of these 30 stress tensors were sorted into four stress phases (P1–P4) using a stress tensor similarity cluster analysis based on angles between stress tensor 9D vectors. The oldest phase is P4 – N–S trending compression. P1 is younger, and responsible for the reactivation of NW–SE striking dextral strike-slip faults. Both are post-Cretaceous pre-Langhian phases. The second-to-last phase is P3 associated with WNW–ESE striking mostly normal faults. This stress state had been active during the Miocene before the Tortonian P2 phase. The last phase is the Tortonian P2 phase, which is characterised by NNE–SSW striking dextral strike-slip faulting.

Keywords: paleostress analysis, multiple inverse method, calcite twinning, Moravian Karst

Introduction

The Moravian Karst is situated E to NE of Brno (SE Moravia, Czech Republic; Fig. 1a). It is an Upper Devonian to Lower Carboniferous Variscan pre-flysch para-autochtonous, mostly carbonate complex overlaying Cadomain igneous rocks of the Brno Massif and underlaying Variscan flysch nappes. The Moravian Karst has a complex Variscan history. It was not only thrust over by the Variscan flysch complex, but even different carbonate facies of the Moravian Karst were juxtaposed: deeper-water Famennian to Visean calciturbiditic facies were thrust over shallower-water facies (comprising micritic and brecciated limestones) of the same age. Carbonate sequences of the Moravian Karst were subsequently (in places) thrust over the Variscan flysch nappes (Kettner 1949; Rez et al. 2011). Late Variscan and Alpine tectonic evolution comprise mainly faulting in extensional, compressional, and strike-slip regimes.

Despite the fact that the deformation history of the Moravian Karst has been a subject of heated discussions for over a century, paleostress analysis is severely lagging behind. Only a handful of manuscripts (theses and mapping reports) deal with it, and only as a side topic. No comprehensive paper on paleostress analysis has ever been published. One can only speculate why, but it is likely due to a combination of complex deformation history and a lack of unweathered outcrops (The Moravian Karst is a preserved area, so there is only a handful of quarries in the area). This lack of data inspired us to investigate alternative sources of data suited for paleostress analysis in the form of calcite twinning, since paleostress analysis based on calcite twinning is not dependent on good quality outcrops and has been a viable paleostress analysis tool for decades (e.g., Friedman & Stearns 1971; Lacombe et al. 1990; Gągała 2009).

The southern part of the Moravian Karst situated roughly northeast of Brno (Fig. 1a) is key to understanding the tectonic evolution of the entire basement of the Variscan flysch nappe complex (e.g., Rez et al. 2011). Despite the fact that it is a preserved area, three major quarries were excavated in the Upper Devonian to Lower Carboniferous limestone complex: the Hády, Lesní and Mokrá quarries (also comprising overlaying Variscan flysch sediments; Fig. 1b), exposing tectonic relationships between pre-flysch and flysch complexes, as well as a detailed tectonic structure of the carbonate pre-flysch complex (for more detail, see Rez et al. 2011). These three quarries were selected because they provide both data types – fault-slip data for "traditional" paleostress analysis and calcite veins for paleostress analysis based on calcite twinning in sufficient numbers and quality. Both types of data were analysed by appropriate available software and their results were compared.

This paper aims to prove the calcite twinning stress inversion as a viable substitute/addition of traditional slick and slide stress analysis, as well as set a benchmark of stress analysis in the Moravian karst and adjacent areas.

Geological setting

Sediments of the Moravian Karst are platform facies of the pre-flysch sequences of the Moravo–Silesian Paleozoic zone, which is regarded as the continuation of the Rhenohercynian zone (Franke 1995; Kalvoda et al. 2002, 2003). These sediments overlay crystalline basements formed by igneous rocks

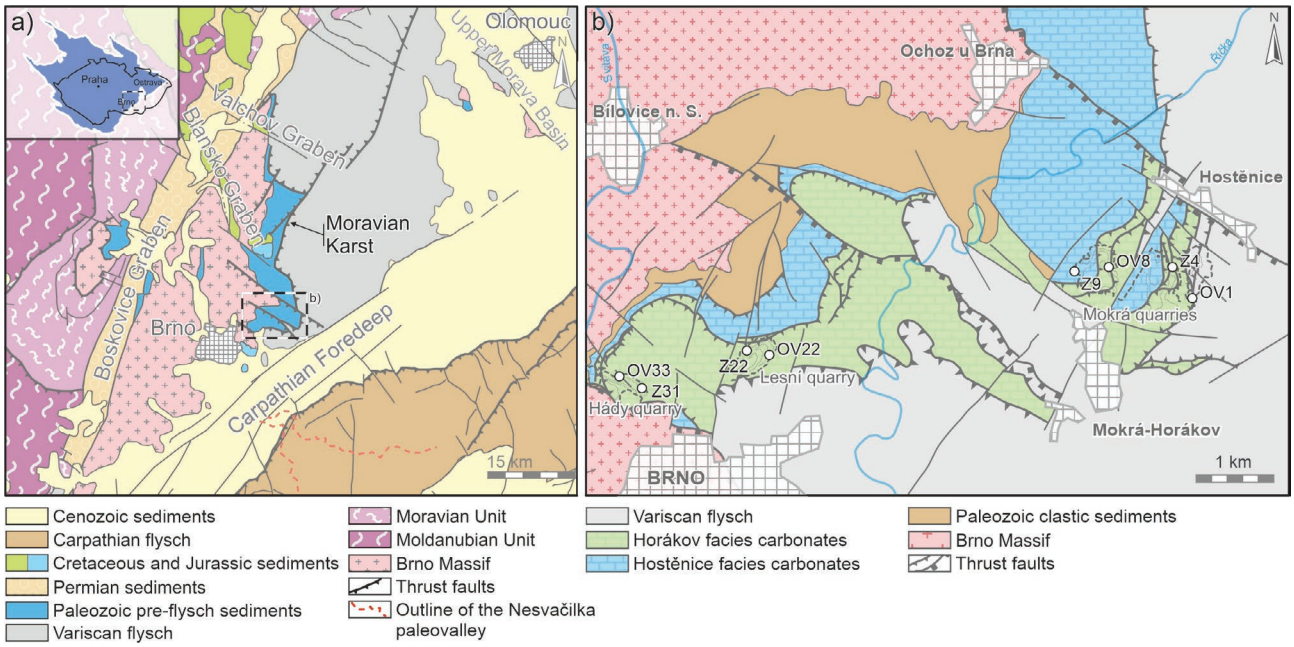

Fig. 1. Geological setting of the southern part of the Moravian Karst: **a** — schematic geological map of the SE part of the Czech Republic (modified after Kodym et al. 1968); **b** — geological sketch of the southern part of the Moravian Karst with highlighted positions of calcite vein samples used in this paper (modified after Rez et al. 2011).

(granitoids and metabasites) of the Brno Massif, which is a part of the Brunovistulian terrane (e.g., Kalvoda et al. 2007). The Brno Massif has a very complex Cadomian, Variscan, and Alpine deformation history (e.g., Hanžl & Melichar 1997; Kalvoda et al. 2007).

The sedimentary sequence of the Moravian Karst comprises Cambrian (in some places south of the Moravian Karst) and Devonian "basal" clastics, mainly arcoses and conglomerates, which are overlain by reefoid carbonates of the Macocha Formation (Zukalová & Chlupáč 1982; Hladil 1983) of Late Eifelian to Frasnian age. These are overlain by the Líšeň Formation (Fammenian to Visean) with more differentiated carbonate facies development reflecting increased subsidence rates and tectonic activity (Prantl 1948; Dvořák 1967; Kalvoda 1995; Kalvoda et al. 1996). This differentiation also affected the uppermost cycle of the underlying Macocha Formation (Hladil 1986). The Líšeň Formation is developed in two distinct facies: shallow water Hostěnice facies and deeper water Horákov facies (Prantl 1948; Hladil et al. 1991). The Hostěnice facies micritic to biomicritic limestones represent the upper slope condensed sedimentation. During the Late Tournaisian to Middle Visean, the deposition of brecciated to sandy limestones superseded the micritic and biomicritic ones. The deeper water Horákov facies represents lower slope sedimentation, which was more varied than the shallower water facies. During the Famenian, dark grey, biodetrital to biomicritic calciturbidites were deposited, followed by mud calciturbidites during the Early Tournaisian as a result of a global eustatic fall (Kalvoda & Kukal 1987). A global eustatic rise in the Middle Tournaisian (Isaacson et al. 1999) resulted in the deposition of platy, biodetrital to biomicritic calciturbidites with cherty concretions or brecciated cherty layers. Late Tournaisian to Middle Visean sedimentation is characterised by alternating limestones, sandstones, and limey shales of the Březina Formation.

Autochtonous, or better said, paraautochtonous sequences of the Moravian Karst, are overthrust by Variscan flysch nappes of the so-called Culmian facies, which are represented in the southern part of the Moravian Karst by Middle Visean Rozstání Formation (greenish shales with graywackes and conglomerates intercalations) and Upper Visean Myslejovice Formation (graywackes and conglomerates).

Paleozoic sedimentary sequences underwent complex Variscan thrusting. Two major phases can be recognised: (1) Flysch nappes were thrust over the pre-flysch sequences of the Moravian Karst. This thrusting also affected the pre-flysch strata, since the facies of the Líšeň Formation was juxtaposed and the deeper-water Horákov facies was thrust over the shallower water Hostěnice facies (Hladil 1991; Hladil et al. 1991; Rez et al. 2011). The thrust zone is well-exposed in the Mokrá quarries and can be observed in boreholes in the southern part of the Moravian Karst (Kalvoda 1989; Rez et al. 2011). (2) Sequences of the Moravian Karst were thrust over the flysch in some places along the eastern margin of the Moravian Karst. This younger thrusting is associated with NE-vergent folds, which also folded the older thrust planes and are oblique to the older thrusts (this is the reason why in some places, Culmian flysch is thrust over the pre-flysch strata and vice versa in others).

This already complex Variscan (and in the case of the Brno Massif, also Cadomian) structure was further complicated by subsequent Late Variscan and Alpine faulting. From the myriad of fault systems (some are discussed later), the two most prominent stand out throughout the eastern part of the Bohemian Massif and Carpathian Foreland: (a) NNE–SSW-trending SE steeply dipping strike-slip faults and (b) WNW–ESE-trending strike-slip faults, steeply dipping to the NE. The orientation of these faults and their relationships to other structures (they also crosscut the Carpathian nappes east of the Moravian Karst) make them some of the youngest fault systems (some of them are still seismically active; see discussion below).

As mentioned previously in the introduction, no systematic paleostress analysis in the Moravian Karst was published because one can only find a handful of manuscripts, which are either diploma or PhD theses at Masaryk University or mapping reports of the Czech Geological Survey. Baldík et al. (2017) performed a paleostress analysis in the northern part of the Moravian Karst, Dvořák & Melichar (2002) estimated paleostress in the northern part of the Moravian Karst based on kink bands. A generalized overview of paleostress and the associated fault systems in the Moravian Karst and adjacent Brno Massif was provided by Hanžl (1996). Additionally, a diploma thesis by Hroza (2003) focused on paleostress analysis in the Brno Massif. Relevant papers from a wider area around the southern part of the Moravian Karst are presented in relevant paragraphs in the discussion.

Methods

Two paleostress analysis applications were used in the data from the Mokrá quarries, both based on a theoretical framework that had built up during recent decades to effectively reconstruct stress-states: TwinCalc (www.eltekto.cz) for calcite twining (Rez & Melichar 2010; Rez 2020) and MARK for fault-slip data (Kernstocková & Melichar 2009; Melichar & Kernstocková 2010; Kernstocková 2011).

Calcite *e*-twinning has been used for stress inversion purposes since the 1950s, because it is the main deformation mechanism at low temperatures, low confining pressures, and low finite strains (<400 °C, 8 %; e.g. De Bresser & Spiers 1997). *E*-plane twinning occurs only if the shear stress τ_i along the glide vector **g** exceeds τ_c (critical resolved shear stress), which has been proven independent from normal stress, the strain rate, as well as temperature, and its magnitude is approximately 10 MPa (e.g. De Bresser & Spiers 1997). This is very handy because in addition to stress orientation and ratio yielded by conventional fault-slip data stress analysis, stress analysis based on calcite twinning can yield differential stress magnitudes as well.

The most common stress inversion technique based on calcite twinning is the Etchecopar method, which was adapted for calcite twins by Laurent and Lacombe (Laurent et al. 1981; Tourneret & Laurent 1990; Parlangeau et al. 2018), which is based on applying 500–1000 randomly-generated, reduced stress tensors [**T**] on data and selecting the one with the best fit using a penalization function f_L. Rez & Melichar (2010) suggested improvements to this method: a total search instead of a random one and the use of a different penalization function (f_R), which was refined in 2020 (Rez 2020) to provide sharper maxima and hence has a better resolution. Both methods are utilized by TwinCalc (Rez 2020), which is a Windows-based application for stress analysis based on calcite twinning; however, the latter was used and its results are presented in this paper.

Traditional methods of stress analysis of fault-slip data were superseded during the last two decades using the multiple inversion method (Yamaji 2000). The main advantage of this method is its handling of heterogeneous data sets: it can be applied directly to heterogeneous data sets without data pre-sorting, which is often biased and presents unacceptable errors. The multiple inversion is based on the premise that any heterogenous data set is a combination of homogenous data sets. Any subset randomly selected from this heterogenous set might be either heterogenous or homogenous (by chance). Stress analysis performed on a subset can consequently yield either a spurious or real solution (reduced stress tensor). Spurious solutions are scattered, whereas real ones tend to cluster. Such clusters of real solutions are becoming more apparent with an increasing number of analysed subsets. It is also desirable to use a constant number of data in the data subsets. The maximum number of these multiple inversions is given by the number of fault-slip data required for an individual stress inversion. Yamaji (Yamaji 2003; Sato & Yamaji 2006) used the "grid search method" based on Angelier's inversion method (Angelier 1984) for subsets of five faults, and later four, giving a total of $\binom{n}{5}$ or $\binom{n}{4}$ solutions (more fault groups mean more calculations, yet more precise results). Clusters of real solutions can be found by using the Watson density function (Yamaji 2000).

Kernstocková and Melichar (Kernstocková & Melichar 2009; Melichar & Kernstocková 2010; Kernstocková 2011) used a different technique of calculating individual solutions in multiple inversions. Instead of a lengthy grid search for every individual data subset, they introduced a direct calculation utilising fault-slip vectors in 9D σ-space. The concept of σ-space was introduced by Fry (1999, 2001) as a 6D parameter space, because the stress tensor is symmetrical and thus has only 6 independent parameters. Kernstocková and Melichar expanded the σ-space into 9D and demonstrated its advantages over the 6D one (Melichar & Kernstocková 2010). Since there are 6 independent parameters in a reduced stress tensor, one can calculate the stress tensor using a set of 6 linear equations. The multiple inversion would then be calculated using 6 fault groups. The number of equations was further reduced to 4 (Kernstocková & Melichar 2009; Melichar & Kernstocková 2010), utilising the advantages of the 9D σ-space geometry.

A simple cluster analysis was carried out using an inbuilt tool in TwinCalc to sort similar phases and to compare calcite twinning and fault slip analysis results. The angle between

stress tensors in 9D sigma space was used as the criterion (Kernstocková & Melichar 2009; Melichar & Kernstocková 2010; Kernstocková 2011; Rez 2020): the lower the angle, the more similar the stress tensors are. This angle is comparable to the angular distance of stress tensor vectors proposed by Yamaji & Sato (2006), but calculated using 9D sigma space utilising its geometrical benefits. Stress tensor 9D vectors are units and the angles between them can be easily calculated as arcus cosine of their scalar products.

Results

Stress analysis based on calcite twinning was carried out using samples of calcite veins, because limestones in the Moravian Karst lack big calcite grains or recrystallized fossils suitable for stress analysis. Samples used for stress analysis had to meet several criteria; mainly mean grain size and low strain. Coarse-grained samples provide an insufficient number of calcite grains, and extremely fine-grained samples are impossible to measure accurately. Highly-strained veins are also not suitable for analysis, since they mainly contain bent *e*-twins, indicating activity along glide systems and heterogenous strain. They are also often clouded by impurities (Fig. 2b), which decrease the accuracy of measurements when using an optical microscope equipped with a universal stage.

Calcite veins in the southern part of the Moravian Karst were studied in detail by Slobodník (Slobodník 2002; Slobodník et al. 2004, 2006). They recognized two main groups of calcite veins based on geochemical and structural data: Variscan "syntectonic" veins (i.e., veins associated with Variscan orogeny and fluids) and post-Variscan veins. The Variscan "syntectonic" veins are usually short, sometimes fibrous, and irregularly-shaped (lenticular, sigmoidal etc.; Slobodník et al. (2006) defined a wide range of different shapes classes), whereas the post-Variscan veins are straight and long with a blocky texture. Both vein groups have a slightly different orientation (Fig. 2c, d), although the post-Variscan cluster better than the Variscan ones.

Based on the requirements listed above, including the orientation of the sampled veins (Fig. 2e), all samples used in this study were post-Variscan. This is also by design, because the Variscan stress field evolution is well-understood (e.g., Rez et al. 2011), whereas the post-Variscan lags behind. Four samples of calcite veins from the Mokrá quarries (OV1, OV8, Z4, and Z9), two from the Lesní quarry (OV21, Z22), and two from the Hády quarry (OV33, Z31) were used for paleostress analysis based on calcite twinning. Calcite twinning data was acquired using an optical microscope equipped with a 5-axes universal stage. Orientations of *c*-axes, as well as all visible systems were measured, and the accuracy was checked using TwinCalc. If any difference between the theoretical and measured angles (between the *c*-axis and twin systems; if there were more than one twin system, also between different twin systems) exceeded 5°, the measurement was repeated. The data was then orthogonalized and glide vectors were calculated (done automatically by TwinCalc). Grain sizes, twin densities, and average twin thicknesses were also measured (the latter two perpendicularly to the twin system, i.e., when tilted in the universal stage). All acquired data were subjected to further analysis. Altogether, all eight samples comprised 361 calcite grains. A basic overview of all samples is shown in Table 1; their location in Fig. 1b. Most of the *e*-plane systems are twinned, and most of the grains have one or two twin systems. Only a fraction of grains have three twin systems or are untwinned (Table 1).

Results of the Etchecopar stress inversion are summarized in Table 2. Initially, 5 stress inversion cycles for each sample were run with the TwinCalc default settings for a rough first look and search parameters testing. Five cycles are the hard coded maximum of stress phases, in which TwinCalc provides for one sample. There are ways around the hard limit (by feeding the residual data set into the cycle again as an independent file); however, this is usually not necessary, since the last stress states tend to be unreliable with exaggerated differential stresses. After this initial round, more detailed searches were run to fine-tune the resulting stress states. Only stress states with considerable numbers of compatible twins (nCT), compatible untwinned *e*-planes (nCU), and low numbers of incompatible untwinned *e*-planes (nIU) were chosen for further analysis. 20 phases from 8 samples met these criteria (Table 2). From the 20 phases, OV8_P2 and OV8_P3 had the worst ratios (less than 2:1) of nCT and nIU; they also have the highest differential stresses, which is the cause of the less favourable nCT/nIU ratio. However, these differential stresses are still the best solutions, and only one of them (OV8_P2) was assigned to a main stress phase. All estimated differential stresses were between 26 and 78 MPa, with a mean value of 45 MPa.

Three datasets from three major quarries in the southern part of the Moravian Karst were acquired. The accuracy of measurements was checked in the field via an excel phone app to prevent any data loss during subsequent processing because generally, only data with small measurement errors (less than 5°) are viable for paleostress analysis (e.g., Kernstocková & Melichar 2009). Thanks to this process, the mean error was only 1.2°±1.5°, which is well within the tolerance of compass measurements. Fault data was analysed using the latest version of MARK (Kernstocková & Melichar 2009; Melichar & Kernstocková 2010; Kernstocková 2011). Results of the paleostress analysis are summarised in Table 3 and Fig. 3. A data set of 52 faults was acquired in the Mokrá quarries. 47 faults were separated into four homogenous data sets (13 faults were compatible with two stress states). Data acquisition in the Lesní quarry yielded 65 faults for analysis, which were separated into 3 homogenous data sets with 6 faults left over (3 faults were compatible with two stress states). And finally, in the Hády quarry, a dataset of 59 faults was acquired, with 51 of them being separated into homogenous data sets (only 1 fault was compatible with two stress states) with 7 faults left over that did not yield any stable paleostress solution.

Discussion

A simple cluster analysis was carried out using TwinCalc to sort similar phases and compare the results of calcite twinning and fault slip analysis. The angle between stress tensors in 9D sigma space was used as the criterion (Kernstocková & Melichar 2009; Melichar & Kernstocková 2010; Rez 2020): the lower the angle, the more similar the stress tensors were. This angle was very similar to the angular distance of stress tensor vectors proposed by Yamaji & Sato (2006), but

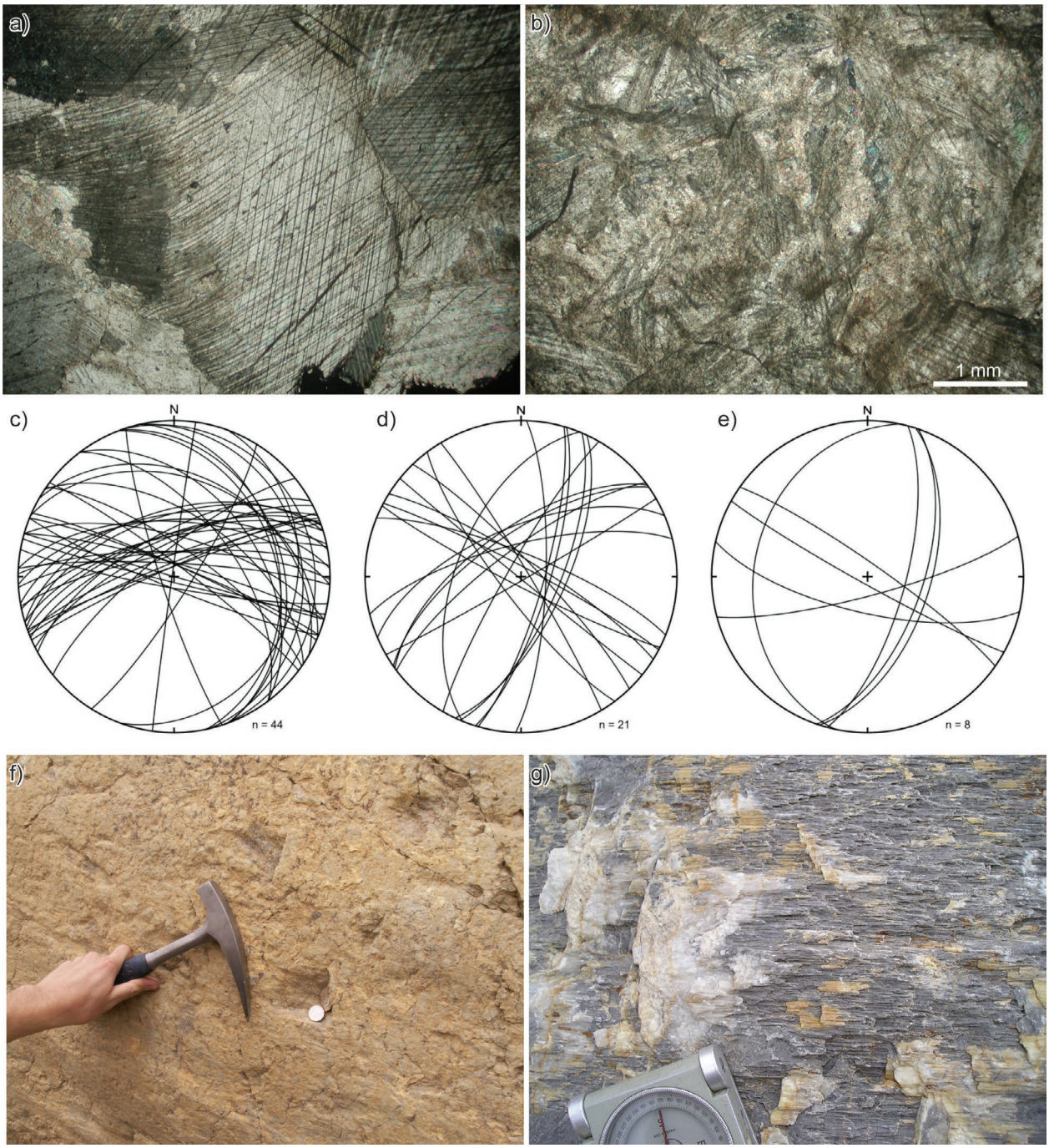

Fig. 2. a — Microphotograph of Z9 sample showing a typical grain of calcite with two sets of twins (I type of lamellae after Ferrill et al. 2004, e.g. thin lamellae with low to moderate densities), crossed polarisers; **b** — Microphotograph of a vein sample not suitable for paleostress analysis – small and cloudy grains; **c** — Equal-area plot of Variscan calcite veins in the southern part of the Moravian Karst (Slobodník et al. 2006); **d** — Equal-area plot of post-Variscan calcite veins in the southern part of the Moravian Karst (Slobodník 2002); **e** — Equal-area plot of veins sampled for this study; **f** — Dextral Riedel shears on a fault plane, Mokrá quarries; **g** — Dextral calcite accretion steps and stylolites on a fault plane, Mokrá quarries.

Table 1: Overview of calcite vein samples basic statistics from the Mokrá quarries.

	Mokrá quarries				Lesní quarry		Hády quarry	
sample	**OV1**	**OV8**	**Z4**	**Z9**	**OV21**	**Z22**	**OV33**	**Z31**
vein orientation	105/70	165/80	209/86	282/28	108/57	193/71	35/83	109/61
number of grains	49	44	25	48	50	49	46	50
twinned e-planes [%]	52.40	54.50	54.70	63.20	58.00	60.54	56.52	52.00
untwinned e-planes [%]	47.60	45.50	45.30	36.80	42.00	39.46	43.48	48.00
grains with no twins [%]	2.04	6.82	0	0	6.90	3.33	0.00	11.54
grains with one set [%]	44.90	31.82	36	10.42	41.38	33.33	57.69	46.15
grains with two sets [%]	46.94	52.27	64	89.58	48.28	56.67	38.46	34.62
grains with three sets [%]	6.12	0.09	0	0	3.45	6.67	3.85	7.69
biggest grain [mm]	2.5	4.1	8.4	6	4.8	3.5	7.4	5.7
smallest grain [mm]	0.21	0.2	0.9	0.1	0.3	0.5	0.7	0.3
mean grain size [mm]	0.85	1.18	3.87	1.22	1.53	0.87	3.25	1.15
standard deviation	0.65	0.98	2.05	1.13	1.24	0.75	1.87	1.02

Table 2: Overview of stress tensors from the Mokrá quarries yielded by calcite twinning analysis (OV1_P1 to Z9_P3). σ_1 to σ_3 are Euler angles of principal stress axes represented by their trend and plunge, Φ is the stress shape ratio($\Phi=(\sigma_2-\sigma_3)/(\sigma_1-\sigma_3)$). Δσ is the differential stress, nCT is the number of compatible twinned *e*-planes, nCU is the number of compatible untwinned *e*-planes and nIU is the number of incompatible, untwinned *e*-planes.

	sample	**σ_1**		**σ_2**		**σ_3**		**Φ**	**Δσ [MPa]**	**nCT**	**nCU**	**nIU**
Mokrá quarries	OV1_P1	347	9	79	15	227	73	0.7	42	35	62	8
	OV1_P2	216	20	56	69	308	7	0.3	36	19	70	0
	OV8_P1	181	60	353	0	85	3	0.4	36	17	57	3
	OV8_P2	281	54	151	25	49	0	0.5	78	37	41	19
	OV8_P3	308	4	45	61	216	29	0.7	62	31	44	16
	Z4_P1	116	61	348	0	250	21	0.7	47	22	32	2
	Z4_P2	351	4	82	12	243	90	0.7	27	8	34	3
	Z9_P1	145	35	39	0	283	47	0.2	43	44	49	4
	Z9_P2	213	38	88	36	331	31	0.81	26	22	53	0
	Z9_P3	263	61	151	12	55	26	0.31	45	12	52	1
Lesní quarry	OV21_P1	355	16	90	14	218	69	0.5	36	30	75	1
	OV21_P2	252	52	142	15	41	34	0.42	53	24	63	2
	OV21_P3	225	26	79	59	322	16	0.78	41	18	48	6
	Z22_P1	266	54	152	16	52	32	0.38	56	38	78	0
	Z22_P2	80	11	350	0	258	79	0.15	37	22	65	3
Hády quarry	OV33_P1	342	34	78	8	180	55	0.6	38	31	68	0
	OV33_P2	238	53	331	2	62	37	0.48	64	25	72	3
	Z31_P1	136	57	344	29	247	13	0.67	40	21	78	1
	Z31_P2	354	64	223	18	127	19	0.5	48	16	53	5
	Z31_P3	221	31	78	53	323	18	0.6	37	8	48	2

Table 3: Overview of stress tensors from the Southern part of the Moravian Karst yielded by multiple stress inversion of fault data. σ_1 to σ_3 are Euler angles of principal stress axes represented by their trend and plunge, Φ is the stress shape ratio ($\Phi=(\sigma_2-\sigma_3)/(\sigma_1-\sigma_3)$).

phase	**σ_1**		**σ_2**		**σ_3**		**Φ**	**compatible faults**
M1	229	45	68	44	329	9	0.76	27
M2	247	51	337	0	67	39	0.27	18
M3	60	34	270	52	160	15	0.05	25
M4	161	35	19	48	266	20	0.93	16
L1	265	41	145	30	33	34	0.55	25
L2	199	40	81	30	327	36	0.64	21
L3	151	51	23	27	278	27	0.53	16
H1	214	28	68	57	313	16	0.45	18
H2	251	31	146	21	29	50	0.35	21
H3	67	44	271	44	169	12	0.4	14

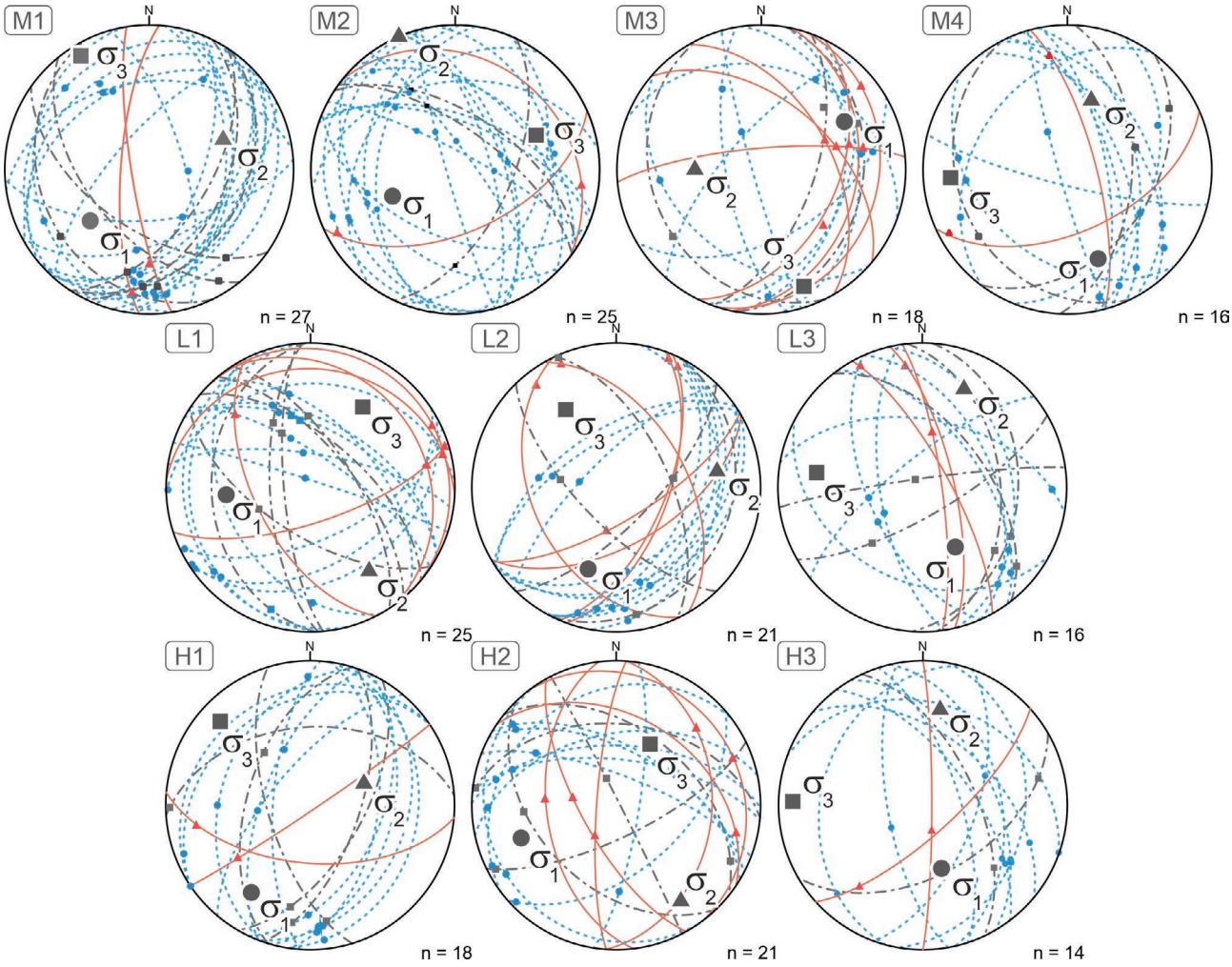

Fig. 3. Results of the fault-slip data paleostress analysis by MARK – homogeneous data sets from the Mokrá quarries (M1–M4), Lesní quarry (L1–L3) and Hády quarry (H1–H3) and respective normal stresses orientation. The blue-dot large circles with a blue circle symbol represent normal to transtensive strike-slip faults, while the red solid lines with red triangle symbols represent reverse to transpresive strike-slip faults. The grey dash-dot lines represent faults without any known shear sense.

calculated using 9D sigma space utilising its geometrical benefits. Stress tensor 9D vectors are units, and the angles between them can be easily calculated as arcus cosine of their scalar products.

A dendrogram of possible stress phases is presented in Fig. 4. 26 out of 30 stress tensors yielded by both paleostress methods were sorted into 4 main paleostress phases, P1 to P4 (Table 4). All clusters have angles between stress vectors less than 50° with two exceptions, OV8_P1 in cluster P1 (52,5°) and H2 in cluster P3 (54°). 50° as a cut-off value may appear too high, but one has to remember that the angle is in 9D. All stress phases cluster nicely in their respective equal-area plots (Fig. 4). A mean stress tensor for each cluster was calculated using eigenvectors and eigenvalues of 9×9 orientation matrices of all stress tensor 9D vectors within each cluster to represent each stress phase. These mean stress tensors are listed in Table 4 and incorporated into equal-area plots in Fig. 4. The fifth phase, which is apparent in the lower part of the dendrogram (Fig. 4), exceeded acceptable angles between individual stress tensors (the lowest is 66°) and was rejected.

One common problem in paleostress analysis is the determination of relative ages of estimated stress states. Typically, multiple striations on one fault plane are used. Unfortunately, no faults with multiple striations with relative timing of striations were found (at least not with a degree of confidence worth publishing). However, NNE–SSW faults are often very planar and almost polished, suggesting multiphase activity.

Stress analysis based on calcite twinning, however, does not provide reliable tools for determining relative timing of stress phases. Theoretically, since *e*-twinning is asymmetrical and can therefore be approximated to simple shear, younger twin systems crossing older ones should indicate relative age of these twin systems. However, the reality is seldom unambiguous. Crossing twins are either too thin to show the asymmetry definitely or the crossing is not clear due to optical "noise" caused either by a localized strain or Rose channels (basically

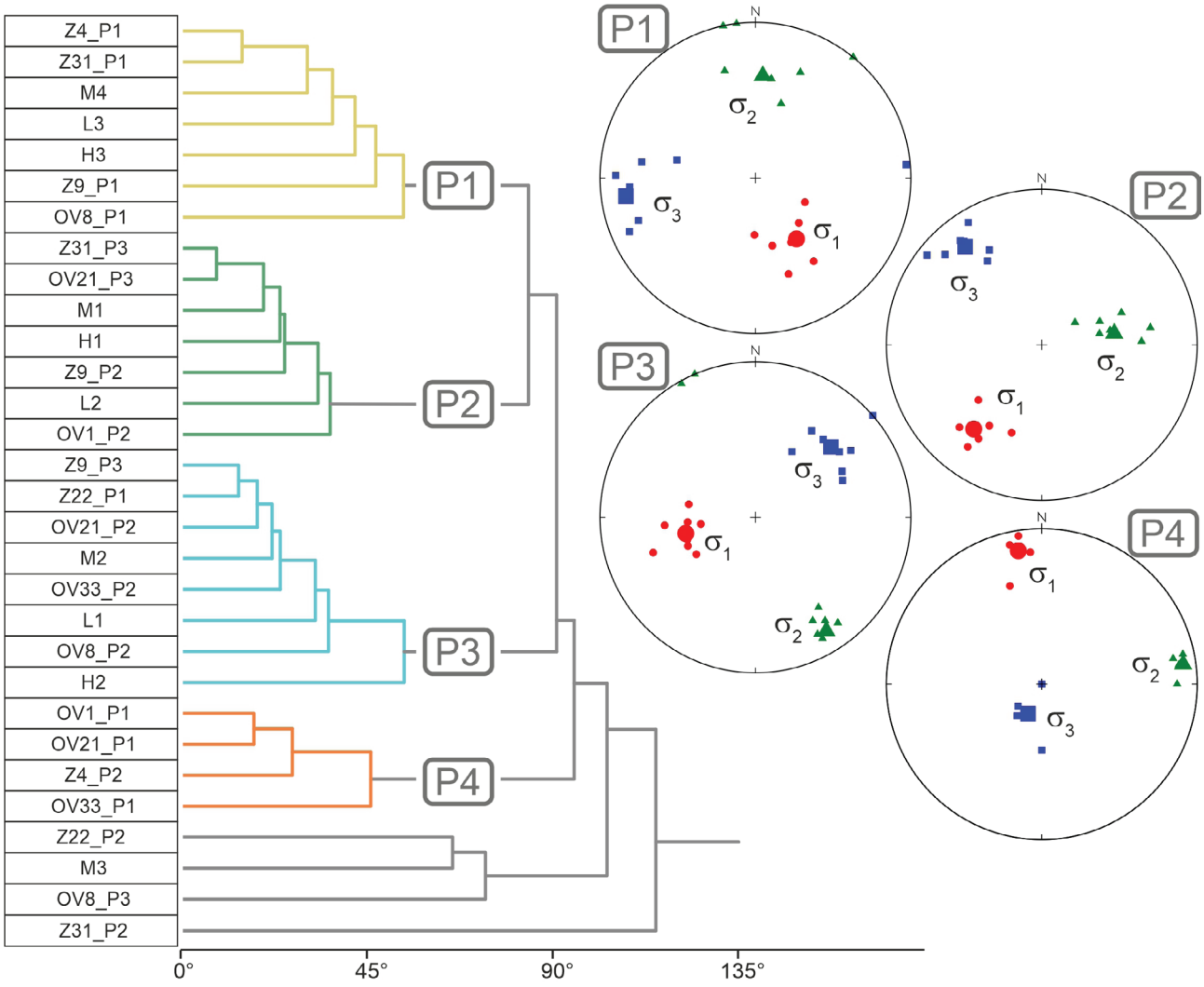

Fig. 4. Results of the stress analysis from the southern part of the Moravian Karst; dendrogram of the cluster analysis and equal area plots of P1, P2, P3, and P4 phases (normal stresses of all stress tensors belonging to the respective phase in smaller symbols, the average orientation in big symbols; equal area projection, lower hemisphere).

Table 4: Overview of the mean stress tensors of phases P1 to P4 from the Southern part of the Moravian Karst. σ_1 to σ_3 are Euler angles of principal stresses, Φ is the stress shape ratio ($\Phi=(\sigma_2-\sigma_3)/(\sigma_1-\sigma_3)$).

phase	σ_1		σ_2		σ_3		Φ
Phase 1	146	51	3	33	260	19	0.57
Phase 2	219	31	81	51	322	21	0.63
Phase 3	257	52	148	15	47	34	0.41
Phase 4	64	38	271	48	165	14	0.23

holes in the lattice). And even if the relative age of twin sets can be determined with some confidence, observations from different grains often contradict each other. Samples used in this study are no exception. Nine twin-sets cross-sections indicate that P2 is older than P3, however, four twin-sets indicate the opposite. Four twin-sets indicate that P1 is older than P3. These findings correspond to the findings presented later in this discussion, but by no means are or should be considered definitive.

Geological context was used to establish relative timing of stress phases yielded by paleostress analysis. The whole area of the southern part of the Moravian Karst is compartmentalised by a network of faults of many deformation phases, so there is plenty to choose from. The two most prominent fault

systems are a system of WNW–ESE, mostly normal faults, and a system of NNE–SSW-oriented normal and strike-slip faults (Fig. 1b). Relative timing of these fault systems is complicated. It seems that the NNE–SSW faults are younger than the WNW–ESE faults. This is supported by the majority of older research (e.g., Dvořák et al. 1987), however, some authors also determined different relative timing of these fault systems (e.g., Hroza 2003). This is consistent with our observations in the field, especially since the NNE–SSW faults are commonly quite planar and almost polished, thereby suggesting multiple reactivations. It is thus quite possible to observe contradictory relative timing indices of these two fault systems in the field.

WNW–ESE faults corresponding to the P3 phase are associated with the Upper Moravia Basin fault system (also called the Nysa–Morava fault system), which is an NW–SE striking system of normal faults (e.g., Špaček et al. 2015).

The NNE–SSW faults of the P2 phase are a lot more complicated, since it is one of the most prevalent fault systems in SE Moravia. These faults have strikes compatible with the Carpathian foredeep and the Vienna basin fault system. The Vienna basin fault system is a sinistral NNE–SSW-striking pull-apart system, which is documented by fault geometry and focal mechanisms (e.g., Fodor 1995; Decker et al. 2005; Hinsch et al. 2005). It cross-cuts both the Carpathian nappes and the eastern part of the underlying Bohemian Massif. Both these fault systems have, however, overall sinistral shear sense, whereas P2 induces dextral strike-slip movements. Nevertheless, both fault systems have complex deformation history, and snippets of evidence of dextral movements along these faults do exist. Peresson & Decker (1997) described dextral transpressional movements in the Vienna Basin fault system during the Pannonian (Tortonian). Unfortunately, their stress state does not match P2 (they proposed rather W–E trending compression). A more matching stress state was presented by Fodor (1995). He described NE–SW-trending Serravallian dextral transpression similar to Peresson & Decker (1997), but also a Middle to Upper Miocene NE–SW-trending strike-slip tectonic regime resulting in a conjugate set of NNE–SSW-striking dextral strike-slip faults and NE–SW-striking sinistral strike-slip faults (Fig. 5c). This tectonic regime matches P2 very nicely, and also the fault set (Fig. 5c) matches the fault set of P2 (Fig. 5b). The next bit of evidence comes from 3D seismic data interpretation from the Nesvačilka Paleovalley (Opletal 2020). The Nesvačilka Paleovalley is a NE–SW-striking Paleogene sinistral pull-apart basin buried beneath the Carpathian foredeep and flysch belt (see the outline in Fig. 1a). The NW part of the valley is cross-cut by the Carpathian foredeep fault system. The fault system is generally considered a sinistral strike-slip system (e.g., Decker et al. 2005). However, the easternmost fault offsets the Nesvačilka aleovalley dextrally (Fig. 5a). This fault affects Burdigalian strata and is therefore younger, i.e., Langhian. Data from this work (P2; Fig. 5b), data by Fodor (1995; Fig. 5c), and faults from geological maps of the Carpathian foredeep (Fig. 5d) bear a striking resemblance. The data also suggest that the fault data sets represent a conjugate system, which explains the presence of both shear senses.

A very similar stress field to P2 was described by Coubal et al. (2015) from the Lusatian fault belt located ca. 150 km NW from the Moravian Karst (α1). Unfortunately, they could not time the stress state more precisely than between the latest Cretaceous and Paleocene.

Homogeneous datasets compatible with P1 mainly contain NNW–SSE faults (Fig. 3). This stress phase is compatible with the main fault system of the Blansko Graben (Fig. 1), which is filled with Cretaceous (Cenomanian) freshwater sediments. This structure is the most south-eastern part of the larger Bohemian Cretaceous Basin, which was subsequently heavily-faulted and compartmentalised into smaller "basins" (e.g., Čech et al. 1980; Šraut 2008). This is also evidenced by drag folding along the main western fault of the Blansko Graben (e.g., Zvejška 1944; Melichar & Čech 1999). A similar stress state to P1 was previously described by Coubal et al. (2015; phase α3). Precise timing of these events is not possible; the faulting took place between the Cretaceous and Miocene, since Miocene strata (Langhian) are not affected by this faulting (Melichar & Čech 1999). Coubal et al. (2015) placed their α3 phase to Late Eocene–Early Oligocene. However, there is no evidence in the Moravian Karst or its vicinity to support such an age of the P1 phase.

The last phase, P4, does not contain any fault-slip paleostress analysis-based stress tensors; therefore, it is harder to associate with regional stress states. When based purely on the orientation of normal stresses of P4, P4 might be compatible with paleostress forming the so-called Valchov Graben (Fig. 1), which is a similar structure to the Blansko Graben. Relative timing of both grabens is unknown, however, the Valchov Graben is more compatible with the overall structure of the eastern part of the Bohemian Cretaceous Basin (e.g., Čech et al. 1980; Šraut 2008) making the Blansko Graben a more localized probably younger structure. This would make P4 the oldest, yet still Alpine, post-Cretaceous structure.

The sequence of stress states yielded by fault-slip analysis and calcite twinning analysis is as follows: The oldest phase is P4, which has a more or less, N–S-trending compression. P1 is younger, and responsible for the reactivation of NW–SE-striking dextral strike-slip faults. The second-to-last phase is the Langhian P2 phase, which is characterised by NNE–SSW-striking dextral strike-slip faulting. The last phase detected in the southern part of the Moravian Karst is Serravallian P3, which is associated with WNW–ESE-striking, mostly normal faults.

As mentioned above, very few published works exist regarding paleostress analysis within the Moravian Karst. Baldík et al. (2017) detected very similar stress states compatible with the P1, P3, and P4 stress phases presented here, but found no evidence for the relative timing of these events. Hroza (2003) detected in his diploma thesis two Alpine stress phases compatible with P2 and P3. Based on intersecting striations that determined the relative timing of these stress states, this is in

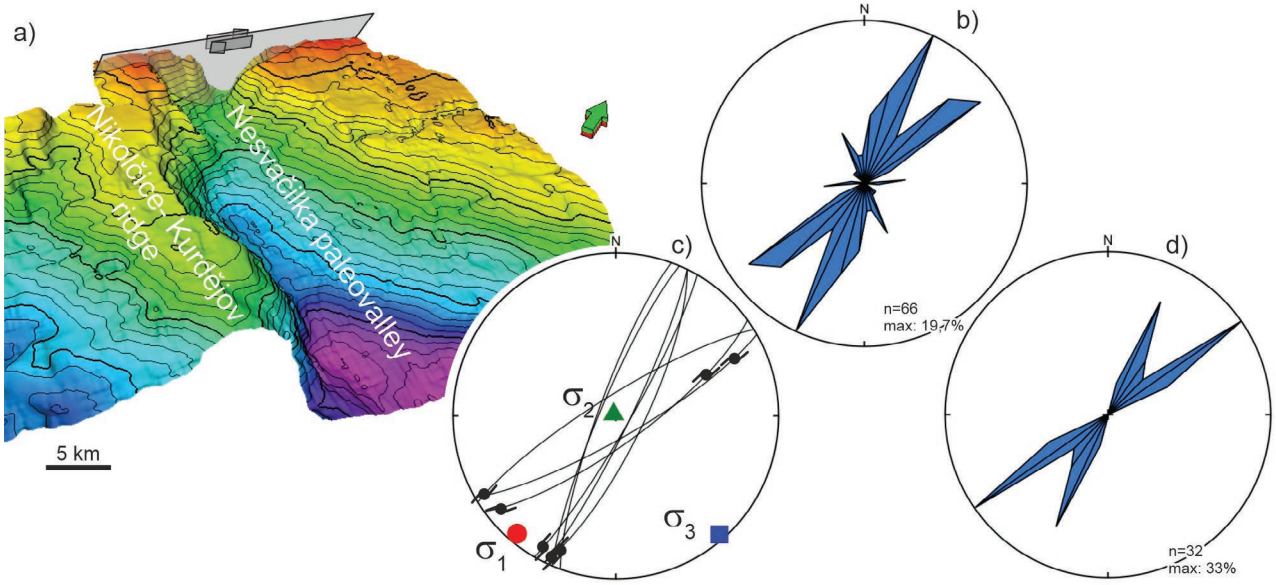

Fig. 5. a — Dextral offset of the NW part of the Nesvačilka Paleovalley (pre-Tertiary surface time interpretation; modified after Opletal 2020); **b** — Rose plot of strikes of all faults compatible with P2 (class size 10°); **c** — Middle to Late Miocene stress state and associated faults by Fodor (1995); equal-area projection, lower hemisphere; **d** — Rose plot of strikes of faults from geological maps of the Carpathian foredeep (class size 10°).

contradiction to our own observations. However, it can be interpreted by long-term simultaneous activity along these two major fault systems, which is still observable to this day. The other works mentioned above dealt with older stress states and do not match the phases presented in this paper.

This tectonic scenario is consistent with tectonic evolution within the Outer Western Carpathian system (e.g., the Carpathian foredeep and the Vienna Basin). Marko et al. (1995) had outlined the tectonic history since the Cretaceous, which was subsequently confirmed and refined by further works (e.g., Fodor 1995; Peresson & Decker 1997; Decker et al. 2005; Salcher et al. 2012; Špaček et al. 2015). They present a very similar sequence of stress states with similar timing. If we use the same names for their stress phases as in this paper, the sequence is as follows: P4, P1, P5, P2, and P3. P5 is a stress state responsible for the Langhian (Badenian) sinistral pull-apart evolution of the Vienna Basin. This phase, however, was not recorded in the data from the southern part of the Moravian Karst.

Conclusions

Paleostress analysis, based on calcite twinning using TwinCalc, yielded 21 stress states using 203 twin systems from 8 samples of calcite veins. Paleostress analysis, based on fault-slip data using MARK, yielded 10 stress states from 176 faults. All stress states were sorted into 4 stress phases (P1–P4) using cluster analysis based on angles between stress tensor 9D vectors.

All four stress states are Alpine, based on geological context and also as a result of a deliberate choice of calcite veins used for the analysis, which are all post-Variscan veins. The oldest stress state is P4, having an almost N-S compression, which is compatible with WNW–ESE-oriented faults of the Valchov Graben and is a post-Cretaceous pre-Burdigalian (Eggenburgian) structure in the northern tip of the Brno Massif (Fig. 1a). The next phase is P1, having more or less N–S transpression, which mainly reactivated the NNW–SSE faults. One of the most prominent structures of this system is the marginal fault of the Blansko Graben, which is a very similar structure to the Valchov Graben, but slightly differently-oriented. This dates P1 also between the Cretaceous and Burdigalian, although P1 is probably younger than P4.

The following stress phase is P2, which is a NE–SW strike-slip stress state. Faults compatible with this phase are compatible directionally with the fault system of the Carpathian Foredeep, but have a dextral rather than sinistral shear sense. Dextral offset of the Nesvačilka Paleovalley observable in 3D seismic suggests that it was a dextral strike-slip system, at least sometimes during the history of this fault system. The faults of the system with the dextral shear-sense, cross-cut Burdigalian strata are therefore younger, probably Langhian.

The last phase is a NE–SW extension P3. It is associated with WNW–ESE-striking mainly normal faults. These faults are associated with the WNW–ESE-striking in the Upper Moravia Basin fault system and are most likely of Serravallian age.

The viability of calcite stress analysis has been proven several times in the past. Excellent correlation of stress states

estimated by inversion of fault-slip and calcite twinning data in the southern part of the Moravian Karst proves calcite twinning paleostress analysis to be a viable substitute for more traditional fault-slip data paleostress analysis in the context of the Moravian Karst and far beyond.

Acknowledgements: This study was supported by project no. SS02030023 – Horninové prostředí a nerostné suroviny „RENS" – Podzemní vody v krasovém systému. Many thanks to Dr. Jiří Faimon for his help with the manuscript and all reviewers for useful suggestions

References

Angelier J. 1984: Tectonic analysis of fault slip data sets. *Journal of Geophysical Research* 89, 5835–5848. https://doi.org/10.1029/JB089iB07p05835

Baldík V., Buriánek D., Čáp P., Franců J., Fürichová P., Gilíková H., Janderková J., Kašperáková D., Kolejka V., Krejčí V., Kryštofová E., Müller P., Novotný R., Otava J., Pecina V., Rez J., Sedláček J., Sedláčková I., Večeřa J. & Vít J. 2017: Vysvětlivky k základní geologické mapě ČR list Ostrov u Macochy 24-233 [Basic geological map 1:25,000, sheet Ostrov u Macochy]. *Manuscript – archive of the Czech Geological Survey* (in Czech).

Coubal M., Málek J., Adamovič J. & Štěpančíková P. 2015: Late Cretaceous and Cenozoic dynamics of the Bohemian Massif inferred from the paleostress history of the Lusatian Fault Belt. *Journal of Geodynamics* 87, 26–49.

Čech S., Klein V., Kříž J. & Valečka J. 1980: Revision of the Upper Cretaceous stratigraphy of the Bohemian Cretaceous Basin. *Věstník Ústředního Ústavu Geologického* 55, 277–296.

De Bresser J.H.P. & Spiers C.J. 1997: Strength characteristics of the *r*, *f* and *c* slip systems in calcite. *Tectonophysics* 272, 1–23. https://doi.org/10.1016/S0040-1951(96)00273-9

Decker K., Peresson H. & Hinsch R. 2005: Active tectonics and Quaternary basin formation along the Vienna Basin Transform Fault. *Quaternary Science Reviews* 24, 305–320. https://doi.org/10.1016/j.quascirev.2004.04.012

Dvořák J. 1967: Vývoj synsedimentárních struktur v jižní části Moravského krasu [Development of synsedimentary structures in the southern part of the Moravian Karst, in Czech]. *Časopis pro mineralogii a geologii* 12, 237–246 (in Czech).

Dvořák V. & Melichar R. 2002: Nástin tektonické stavby severní části Moravského krasu [Outline of tectonic evolution of the northern part of the Moravian Karst, in Czech]. *Geologické výzkumy na Moravě a ve Slezsku v roce 2001*, 51–54.

Dvořák J., Friáková O., Hladil J., Kalvoda J. & Kukal Z. 1987: Geology of the Palaeozoic rocks in the vicinity of the Mokrá Cement Factory quarries, Moravian Karst. *Sborník geologických věd, Geologie* 42, 41–88.

Ferrill D.A., Morris A.P., Evans M.A., Burkhard M., Groshong R.H. & Onasch C.M. 2004: Calcite twin morphology: a low-temperature deformation geothermometer. *Journal of Structural Geology* 26, 1521–1529. https://doi.org/10.1016/j.jsg.2003.11.028

Fodor L. 1995: From transpression to transtension: Oligocene–Miocene structural evolution of the Vienna Basin and the East Alpine–Western Carpathian junction. *Tectonophysics* 242, 151–182. https://doi.org/10.1016/0040-1951(94)00158-6

Franke W. 1995: III. B. 1. Stratigraphy. In: Dallmayer R.D., Franke W. & Weber K. (Eds.): Pre-Permian geology of Central and Eastern Europe. *Springer*, 33–49.

Friedman M. & Stearns D.W. 1971: Relations between stresses inferred from calcite twin lamellae and macrofractures, Teton anticline, Montana. *Geological Society of America Bulletin* 82, 3151–3162. https://doi.org/10.1130/0016-7606(1971)82[3151:RBSIFC]2.0.CO;2

Fry N. 1999: Striated faults: visual appreciation of their constraint on possible paleostress tensors. *Journal of Structural Geology* 21, 7–21. https://doi.org/10.1016/S0191-8141(98)00099-6

Fry N. 2001: Stress space: striated faults, deformation twins, and their constraints on paleostress. *Journal of Structural Geology* 23, 1–9. https://doi.org/10.1016/S0191-8141(00)00136-X

Gągała Ł. (2009): Reliability of selected procedures of stress inversion and data separation for inhomogeneous populations of calcite twins and striated faults: insights from numerical experiments. *International Journal of Earth Sciences* 98, 461–479. https://doi.org/10.1007/s00531-007-0262-3

Hanžl P. 1996: Geologický profil mezi Čebínem a Skalním mlýnem [Geological profile between Čebín and Skalní mlýn]. *PhD thesis, Faculty of science, Masaryk University*, Brno (in Czech).

Hanžl P. & Melichar R. 1997: The Brno Massif: a section through the active continental margin or a composed terrane? *Krystalinikum* 23, 33–58.

Hinsch R., Decker K. & Wagreich M. 2005: A short review of Environmental Tectonics of the Vienna Basin and the Rhine Graben area. *Austrian Journal of Earth Sciences* 97, 6–15.

Hladil J. 1983: Cyklická sedimentace v devonských karbonátech macošského souvrství [Cyclic sedimentation of Devonian carbonates of the Macocha Formation]. *Zemní plyn a nafta* 28, 1–15 (in Czech).

Hladil J. 1986: Trends in the development and cyclic patterns of Middle and Upper Devonian buildups. *Facies* 15, 1–33. https://doi.org/10.1007/BF02536716

Hladil J. 1991: Násunové struktury jižního uzávěru Moravského krasu, 24-413 Mokrá-Horákov [Thrust structures in the southern closure of the Moravian Karst, 24-413 Mokrá-Horákov]. *Zprávy o geologických výzkumech v roce 1989*, 80–81 (in Czech).

Hladil J., Krejčí Z., Kalvoda J., Ginter M., Galle A. & Berousek P. 1991: Carbonate ramp environment of Kellwasser time-interval, Lesní lom, Moravia, Czechoslovakia. *Bulletin de la Societe geologique de Belgique* 100, 57–119.

Hroza M. 2003: Paleonapjatostní analýza vybraných lokalit brněnského masivu [Paleostress analysis of selected sites in the Brno Massif]. *Diploma thesis, Department of Geological Sciences, Masaryk University*, Brno (in Czech).

Isaacson P.E., Hladil J., Shen J.W., Kalvoda J. & Grader G. 1999: Late Devonian Famennnian glaciation in South America and marine offlap on other continents. *Abhandlungen der Geologischen Bundesanstalt* 54, 239–257.

Kalvoda J. 1989: Foraminiferová zonace svrchního devonu a spodního karbonu moravskoslezského paleozoika [Foraminifera zonation of the Upper Devonian and Lower Carboniferous of the Moravosilezian Zone]. *PhD thesis, Department of Geological Sciences, Masaryk University*, Brno (in Czech).

Kalvoda J. 1995: Devonské pánve při okraji východní Avalonie na Moravě [Devonian basins at the eastern margin of Avalonia]. *Geologické výzkumy na Moravě a ve Slezsku v roce 1994*, 48–50 (in Czech).

Kalvoda J. & Kukal Z. 1987: Devonian-Carboniferous boundary in the Moravian Karst at Lesní lom Quarry, Brno-Líšeň, Czechoslovakia. *Courier Forschundinstitut Senckenberg* 98, 95–117.

Kalvoda J., Bábek O., Nehyba S. & Špaček P. 1996: Svrchnodevonské a spodnokarbonské kalciturbidity z Lesního lomu v Brně-Líšni (jižní část Moravského krasu) [Upper Devonian and Lower Carboniferous calciturbidites from the Lesní lom quarry in Brno-Líšeň (southern part of the Moravian Karst)]. *Geologické výzkumy na Moravě a ve Slezsku v roce 1995*, 98–100 (in Czech).

Kalvoda J., Melichar R., Bábek O. & Leichmann J. 2002: Late Proterozoic–Paleozoic tectonostratigraphic development and paleogeography of Brunovistulian Terrane and comparison with other terranes at the SE margin of Baltica-Laurussia. *Journal of the Czech Geological Society* 47, 81–102.

Kalvoda J., Leichmann J., Bábek O. & Melichar R. 2003: Brunovistulian Terrane (Central Europe) and Istanbul Zone (NW Turkey): Late Proterozoic and Paleozoic tectonostratigraphic development and paleogeography. *Geologica Carpathica* 54, 139–152.

Kalvoda J., Bábek O., Fatka O., Leichmann J., Melichar R., Nehyba S. & Špaček P. 2007: Brunovistulian terrane (Bohemian Massif, Central Europe) from late Proterozoic to late Paleozoic: a review. *International Journal of Earth Sciences* 97, 497–518. https://doi.org/10.1007/s00531-007-0183-1

Kernstocková M. 2011: Paleonapjatostní analýza polyfázově reaktivovaných zlomů na příkladu barrandienu [Paleostress analysis of polyphase reactivated faults in the Barrandien area]. *PhD thesis, Department of Geological Sciences, Masaryk University*, Brno (in Czech).

Kernstocková M. & Melichar R. 2009: Numerical Paleostress Analysis – Limits of Automation. *Trabajos De Geologia* 29, 399–403.

Kettner R. 1949: Geologická stavba severní části Moravského krasu a oblastí přilehlých [Geologic structure of the northern part of the Moravian Karst, in Czech]. *Rozpravy Československé Akademie Věd a Umění*, Třida II 59, 1–29.

Kodym O., Fusán O. & Matějka A. 1968: Geologická mapa ČSSR (odkrytá) [Geological map of ČSSR, in Czech]. *Czech Geological Survey*.

Lacombe O., Angelier J., Laurent P., Bergerat F. & Tourneret C. 1990: Joint analyses of calcite twins and fault slips as a key for deciphering polyphase tectonics: Burgundy as a case sample. *Tectonophysics* 182, 279–300. https://doi.org/10.1016/0040-1951(90)90168-8

Laurent P., Bernard P., Vasseur G. & Etchecopar A. 1981: Stress tensor determination from the study of *e* twins in calcite. A linear programming method. *Tectonophysics* 78, 651–660. https://doi.org/10.1016/0040-1951(81)90034-2

Marko F., Plašienka D. & Fodor L. 1995: Meso-cenozoic tectonic stress fields within the Alpine-Carpathian transition zone: A review. *Geologica Carpathica* 46, 19–27.

Melichar R. & Čech S. 1999: Blansko – Dolní Lhota. *Geolines*, 8, 90 (in Czech).

Melichar R. & Kernstocková M. 2010: 9D Space – The Best Way to Understand Paleostress Analysis. *Trabajos De Geologia* 30, 69–74.

Opletal V. 2020: Geological setting of the South-Eastern slopes of Bohemian massif based on interpretation of petroleum exploration subsurface dataset. *PhD thesis, Masaryk University Brno*.

Parlangeau C., Lacombe O., Schueller S. & Daniel J.M. 2018: Inversion of calcite twin data for paleostress orientations and magnitudes: A new technique tested and calibrated on numerically-generated and natural data. *Tectonophysics* 722, 462–485. https://doi.org/10.1016/j.tecto.2017.09.023

Peresson H. & Decker K. 1997: The Tertiary dynamics of the northern Eastern Alps (Austria): changing palaeostresses in a collisional plate boundary. *Tectonophysics* 272, 125–157. https://doi.org/10.1016/S0040-1951(96)00255-7

Prantl F. 1948: Stratigraficko-paleontologický výzkum devonu na Hádech u Brna [Stratigraphical and paleontological research of the Devonian on the Hády hill near Brno]. *Věstník Státního Geologického Ústavu ČSR* 23, 173–180 (in Czech).

Rez J. 2020: TwinCalc: A multitool for calcite twinning based stress analysis. *Applied Computing and Geosciences* 5, 100020. https://doi.org/10.1016/j.acags.2020.100020

Rez J. & Melichar R. 2010: Peek Inside the Black Box of Calcite Twinning Paleostress Analysis. *Trabajos De Geologia* 30, 163–168.

Rez J., Melichar R. & Kalvoda J. 2011: Polyphase deformation of the Variscan accretionary wedge: an example from the southern part of the Moravian Karst (Bohemian Massif, Czech Republic). In: Poblet J. & Lisle R.J. (eds.): Kinematic Evolution and Structural Styles of Fold-and-Thrust Belts. *Geological Society*, London, 223–235. https://doi.org/10.1144/SP349.12

Salcher B.C., Meurers B., Decker K., Hölzel M. & Wagreich M. 2012: Strike-slip tectonics and Quaternary basin formation along the Vienna Basin fault system inferred from Bouguer gravity derivatives. *Tectonics* 31. https://doi.org/10.1029/2011TC002979

Sato K. & Yamaji A. 2006: Embedding stress difference in parameter space for stress tensor inversion. *Journal of Structural Geology* 28, 957–971. https://doi.org/10.1016/j.jsg.2006.03.004

Slobodník M. 2002: Hydrotermální žilné mineralizace v Moravskérn krasu, Morava, ČR: pohled z hlediska charakteru fluid a P–T podmínek [Hydrothermal mineralisation in the Moravian Karst, Moravia, Czech Republic: insight from type of fluids and p–T conditions point of view]. *Acta Musei Moraviae, Sci. geol.* 87, 113–136 (in Czech).

Slobodník M., Hurai V., Pudilová M. & Král J. 2004: P–T podmínky násunové deformace a charakter generovaných fluid v hádsko–říčských vápencích na Hádech u Brna [P–T conditions during thrusting and character of generated fluids in the Hády–Říčka Limestone on Hády hill near Brno]. *Geologické výzkumy na Moravě a ve Slezsku v roce 2003*, 62–66 (in Czech).

Slobodník M., Muchez P., Král J. & Keppens E. 2006: Variscan veins: record of fluid circulation and Variscan tectonothermal events in Upper Palaeozoic limestones of the Moravian Karst, Czech Republic. *Geological Magazine* 143, 491–508. https://doi.org/10.1017/S0016756806001981

Špaček P., Bábek O., Štěpančíková P., Švancara J., Pazdírková J. & Sedláček J. 2015: The Nysa–Morava Zone: an active tectonic domain with Late Cenozoic sedimentary grabens in the Western Carpathians' foreland (NE Bohemian Massif). *International Journal of Earth Sciences* 104, 963–990. https://doi.org/10.1007/s00531-014-1121-7

Šraut B. 2008: Tektonická stavba východní části české křídové pánve [Tectonics of the eastern part of the Bohemain Cretaceous basin]. *Diploma thesis, Department of geological sciences, Masaryk University*, Brno (in Czech).

Tourneret C. & Laurent P. 1990: Paleo-stress orientations from calcite twins in the North Pyrenean foreland, determined by the Etchecopar inverse method. *Tectonophysics* 180, 287–302.

Yamaji A. 2000: The multiple inverse method: a new technique to separate stresses from heterogeneous fault-slip data. *Journal of Structural Geology* 22, 441–452. https://doi.org/10.1016/S0191-8141(99)00163-7

Yamaji A. 2003: Are the solutions of stress inversion correct? Visualization of their reliability and the separation of stresses from heterogeneous fault-slip data. *Journal of Structural Geology* 25, 241–252. https://doi.org/10.1016/S0191-8141(02)00021-4

Yamaji A. & Sato K. 2006: Distances for the solutions of stress tensor inversion in relation to misfit angles that accompany the solutions. *Geophysical Journal International* 167, 933–942.

Zukalová V. & Chlupáč I. 1982: Stratigrafická klasifikace nemetamorfovaného devonu moravskoslezské oblasti [Stratigraphic classification of unmetamorphosed Devonian of the Moravo–Silesian Zone]. *Časopis pro mineralogii a geologii* 9, 225–247 (in Czech).

Zvejška F. 1944: Blanenský prolom [Blansko Graben]. *Práce Moravské přírodovědecké společnosti* 16, 1–29 (in Czech).